Adoption of a turn conformation drives the binding affinity of p53 C-terminal domain peptides to 14-3-3σ

ACS chemical biology

Articles

Cite This: ACS Chem. Biol. 2020, 15, 262−271

Adoption of a Turn Conformation Drives the Binding Affinity of p53 C-Terminal Domain Peptides to 14-3-3σ

Ave Kuusk,[†,‡,◆] João Filipe Neves,[§,◆] Kenny Bravo-Rodriguez,[∥,⊥,◆] Anders Gunnarsson,[†] Yasser B. Ruiz-Blanco,[∥] Michael Ehrmann,[⊥] Hongming Chen,[†,#] Isabelle Landrieu,[*,§] Elsa Sanchez-Garcia,[*,∥] Helen Boyd,[*,●] Christian Ottmann,[*,‡,▽] and Richard G. Doveston[*,○]

[†]Discovery Sciences, IMED Biotech Unit, AstraZeneca, Mölndal, Sweden

[‡]Laboratory of Chemical Biology, Department of Biomedical Engineering, and Institute for Complex Molecular Systems, Eindhoven University of Technology, Eindhoven, The Netherlands

[§]Lille University, UMR 8576 CNRS, 59000 Lille, France

[∥]Department of Computational Biochemistry, Center of Medical Biotechnology, and [⊥]Department of Microbiology, and [▽]Department of Chemistry, University of Duisburg, Essen, Germany

[#]Chemistry and Chemical Biology Centre, Guangzhou Regenerative Medicine and Health-Guangdong Laboratory, Guangzhou, China

[●]Clinical Pharmacology and Safety Sciences, R&D, AstraZeneca, Cambridge, U.K.

[○]Leicester Institute of Structural and Chemical Biology and School of Chemistry, University of Leicester, University Road, Leicester LE1 7RH, U.K.

Supporting Information

ABSTRACT: The interaction between the adapter protein 14-3-3σ and transcription factor p53 is important for preserving the tumor-suppressor functions of p53 in the cell. A phosphorylated motif within the C-terminal domain (CTD) of p53 is key for binding to the amphipathic groove of 14-3-3. This motif is unique among 14-3-3 binding partners, and the precise dynamics of the interaction is not yet fully understood. Here, we investigate this interaction at the molecular level by analyzing the binding of different length p53 CTD peptides to 14-3-3σ using ITC, SPR, NMR, and MD simulations. We observed that the propensity of the p53 peptide to adopt turn-like conformation plays an important role in the binding to the 14-3-3σ protein. Our study contributes to elucidate the molecular mechanism of the 14-3-3−p53 binding and provides useful insight into how conformation properties of a ligand influence protein binding.

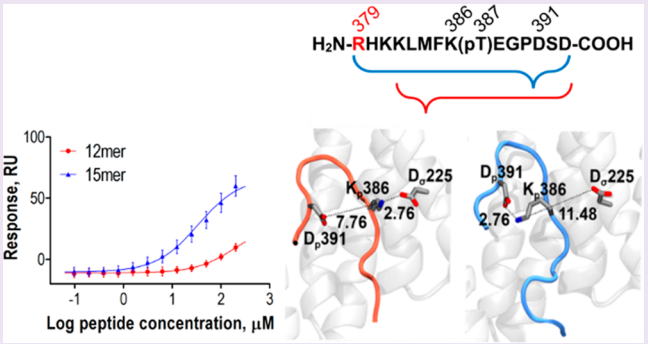

INTRODUCTION

The tumor suppressor protein p53 plays an important role in the cellular response to DNA damage.[1,2] Activation of p53 upregulates genes involved in cell cycle arrest, DNA repair, senescence, and apoptosis.[3,4] Mutations to p53 occur by several mechanisms and are observed in 50% of all human cancers. These can lead to inactivation of p53 and tumor growth.[5,6] In the remaining cancers, p53 is not mutated, but its activity is suppressed by other mechanisms.[1]

14-3-3 proteins belong to a family of highly conserved adapter proteins present in all eukaryotic cells.[7,8] In mammals, seven isoforms with sequence differences in discrete regions have been described: β, γ, ε, ζ, η, τ, and σ.[9] 14-3-3 proteins bind to phosphoserine and phosphothreonine motif-containing proteins and regulate their subcellular localization, enzymatic activity, or interaction with other proteins.[9,10] Of all the isoforms, 14-3-3σ has been directly linked to tumor formation and is down-regulated in several types of malignancy including breast, gastric, prostate, lung, and ovarian cancers.[11−13] 14-3-3σ is a positive regulator of p53; its overexpression inhibits the growth of oncogene-expressing cells in nude mice and reduces the transformation and growth of breast cancer cells.[14,15] In response to DNA damage, the C-terminal domain (CTD) of p53 becomes phosphorylated and interacts with the amphipathic binding groove of 14-3-3 σ[14] This interaction protects p53 from MDM2-mediated proteosomal degradation, resulting in a stabilization of p53 protein levels, an increase in p53 transcriptional activity, and cell cycle arrest.[14−16] Other

Received: November 4, 2019
Accepted: November 19, 2019
Published: November 19, 2019

DOI: 10.1021/acschembio.9b00893
ACS Chem. Biol. 2020, 15, 262−271

14-3-3 isoforms interact with p53 to potentiate its transcriptional activity by facilitating p53 tetramization and thus DNA binding.[16,17] Therefore, stabilization of the 14-3-3−p53 protein−protein interaction (PPI) has potential as a therapeutic strategy for cancer.

14-3-3 binds partner proteins containing recognition motifs that can be classified as mode 1 (RSXpSXP), mode 2 (RXF/YXpSXP), or mode 3 (pS/TX$_{1-2}$-COOH) (pS representing phosphoserine, X representing any amino acid, and −COOH the C-terminus).[18,19] The interaction of 14-3-3 with p53 involves phosphorylation of S378, S366, or T387 residues within the CTD of p53, where T387 is most important (Figure 1).[16,17] Crystallographic analysis has shown that p53 binds to

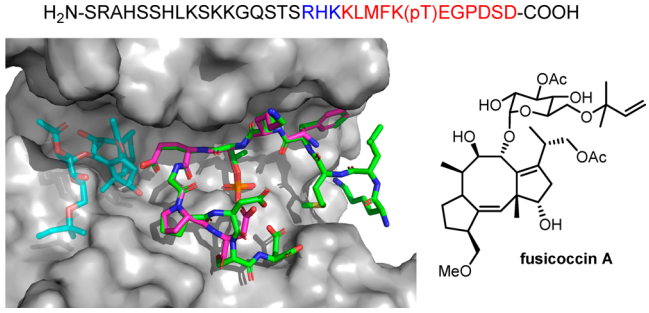

Figure 1. Top: p53 CTD sequence. pT387 is numbered. The 12mer peptide is shown in red. The three additional residues present in the 15mer are shown in blue. Left: Overlay of the binary crystal structures of a p53 9mer peptide (pink sticks, PDB ID: 3LW1) and a p53 12mer peptide (green sticks, PDB ID: 5MOC) bound to the binding channel of 14-3-3σ (gray surface). The binding pose of FC-A is indicated (faded cyan sticks, overlaid from PDB ID: 5MXO). Right: Structure of fusicoccin A.

14-3-3σ via a recognition motif that is different from the classical models.[20] The binary crystal structure of 14-3-3σ in complex with the CTD 9mer peptide of p53 showed that the glycine residue at position +2 of the phosphorylated threonine followed by a proline at position +3 caused a kink in the peptide backbone, resulting in the peptide adopting a turn conformation when bound to 14-3-3σ (Figure 1). The extreme C-terminus of the p53 peptide is engaged in a salt-bridge with an arginine of 14-3-3σ, and consequently, it occupies only around 2/3 of the 14-3-3σ peptide-binding channel. This creates an interface pocket that is able to accommodate a small-molecule PPI stabilizer (Figure 1).[20] In 2017, we provided the first evidence that this pocket could indeed be targeted with small molecules showing that fusicoccin-A acts as a stabilizer for the 14-3-3−p53 PPI.[21]

During our studies of the 14-3-3−p53 PPI, we observed that the length of peptide used to mimic the p53 CTD had a significant and surprising effect on binding affinity. Here, we report the results of a comprehensive study into the effect of p53 peptide length on binding to 14-3-3. The binding affinities of 9mer, 12mer, 14mer, 15mer, 20mer, and 32mer p53 peptides, with phosphorylation at T387, were determined using isothermal titration calorimetry (ITC) and surface plasmon resonance (SPR) assays. The biophysical data demonstrated that the 15mer peptide binds the 14-3-3 protein considerably more tightly as compared to the 12mer peptide, which did not show any binding affinity. This was surprising because the 12mer was present in binary complexes successfully used for protein crystallography. Nuclear magnetic resonance (NMR) analyses and molecular dynamics (MD) simulations were performed to further provide a rationale for this observation. The analysis of these data indicates that the binding affinities of the peptides are related to the disordered character of p53 and its propensity to adopt a turn structure in its bound and unbound states. This finding is important because of two reasons: First, in vitro protein−peptide binding assays are an important screening tool and must provide a reliable indication of affinity—therefore any potential for variability needs to be fully understood. Second, a precise molecular understanding of a protein−peptide interaction is essential for the design of novel and selective stabilizers that target interface pockets.

RESULTS AND DISCUSSION

Analysis of Peptide Binding Affinity to 14-3-3 by ITC and SPR. ITC experiments were performed to measure the thermodynamic characteristics of the 14-3-3σ−p53 PPI and to compare the dissociation constants (K_d) of p53 peptides of different lengths to 14-3-3σ. The thermodynamic parameters and K_d's obtained for the phosphorylated peptides of different lengths are summarized in Figure 2 (see also Figure S1). This data revealed that both 9mer and 12mer peptides do not show any detectable binding to the protein, while the 14mer peptide has a low affinity with a K_d = 120 μM. Binding of the 15mer, 20mer, and 32mer peptides to 14-3-3σ was characterized by K_d's in the same order of magnitude: 25.7, 61.0, and 13.6 μM, respectively. The three additional positively charged amino acid residues (R379, H380, and K381) at the N-terminus of the 15mer peptide thus have a significant positive effect on the binding affinity to 14-3-3σ (Figure 1). Consideration of the thermodynamic parameters (ΔH, $T\Delta S$) showed that binding of the lower affinity 14mer peptide is driven mainly by entropic contributions ($T\Delta S$), likely associated with the formation of hydrophobic interactions upon binding to 14-3-3σ (Figure 2b). In contrast, the higher affinity peptides (15mer and 32mer) bind to 14-3-3σ with a larger enthalpy contribution to the total free energy change. Indeed, the deletion of R379 alone remarkably reduced the binding affinity of the 14mer peptide, to a K_d of 120 μM, predominantly as a result of a decreased enthalpy contribution (ΔH). This suggested the possibility that the interactions with the 15mer and 32mer involved an increased contribution from hydrogen-bonding and/or electrostatic characteristics.

To confirm and further characterize the binding data obtained by ITC, a surface plasmon resonance (SPR) assay was employed that measured binding of the peptides to 14-3-3ζ protein covalently immobilized on the sensor surface. K_d's measured by SPR were in a good agreement with the values determined by ITC (Figure 2a,c), confirming the ranking of affinity with respect to peptide length and the positive effect of the R379 peptide residue on the binding affinity to the protein.

NMR Spectroscopy of the p53 Peptide-14-3-3$\sigma\Delta$C17 Complexes. The K_d values linked to various lengths of p53 peptides could not be directly rationalized from the crystal structure of 14-3-3σ with the 12-mer, and it was not possible to obtain crystal structures of 14-3-3σ complexes with any of the longer peptides. Therefore, an NMR analysis of the complexes formed by $^{15}N^{13}C^{2}H$ labeled C-terminally truncated 14-3-3σ (14-3-3$\sigma\Delta$C17) and p53 CTD peptides was initiated. 2D $^{1}H-^{15}N$ HSQC spectra of 14-3-3$\sigma\Delta$C17 were recorded in the presence and absence of each p53 peptide in order to get further insights on the complex formation. The experiments

DOI: 10.1021/acschembio.9b00893
ACS Chem. Biol. 2020, 15, 262−271

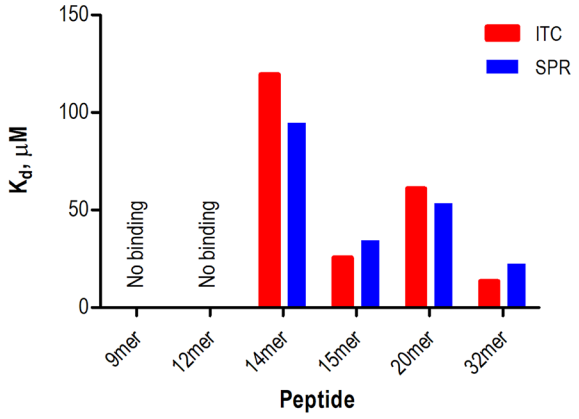

Peptide	K_d ITC, μM	K_d SPR, μM
9mer	-	-
12mer	-	-
14mer	119.6	94.7
15mer	25.7	34.4
20mer	61	53.3
32mer	13.6	22.3

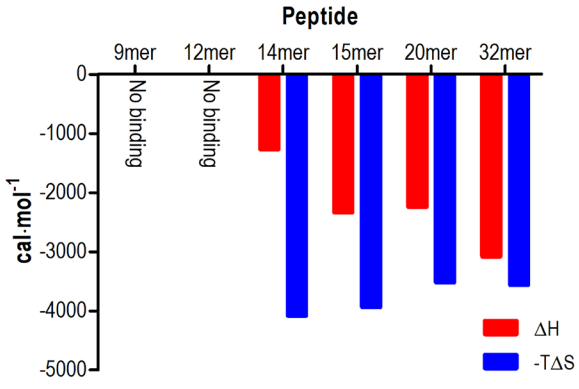

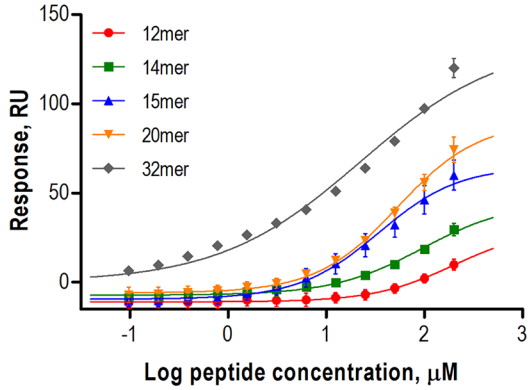

Figure 2. (a) Dissociation constants obtained by ITC and SPR. (b) Thermodynamic parameters obtained by ITC. (c) SPR dose−response curves of 12mer, 14mer, 15mer, 20mer, and 32mer peptides of p53. Data shown are representative of three separate experiments.

were performed for the 12mer, 14mer, 15mer, 20mer, and 32mer, all at a molar stoichiometry of 1:2.5 for 14-3-3σΔC17:peptide. The intensities of the correlation peaks corresponding to specific amino acid residues along the 14-3-3σΔC17 sequence (I) were monitored in NMR spectra of 14-3-3σΔC17 in the presence of each peptide and compared to the intensities of the same correlation peaks in the spectrum of 14-3-3σΔC17 alone (I0).

The addition of each p53 peptide led to peak broadening for a discrete number of resonances in the spectra of 14-3-3σΔC17 (Figures 3 and S2). The intensities of resonances corresponding to amino acid residues remote from the peptide binding channel remained unaffected and similar to the control spectrum ($I/I_0 \approx 1$) (Figures 3a,c and S3). In contrast, the I/I_0 ratio of resonances corresponding to amino acid residues located in, or close, to the phospho-anchoring region of the amphipathic binding groove decreased (Figures 3b,d and S3). Figure 3b illustrates that the magnitude of the decrease of the I/I_0 ratio of the affected peaks was different, depending on the added peptide. The I/I_0 decrease was higher when the protein was exposed to the 32mer, followed by the 15mer, the 20mer, the 14mer, and finally by the 12mer. This series reversely correlates with the measured binding affinities, with the lowest K_d for the 32mer inducing the highest decrease of intensity. This is not unexpected as the magnitude of the broadening of correlation peak intensities, and therefore the drop of the I/I_0 ratio, is proportionally correlated with the amount of 14-3-3σΔC17 bound to peptide in solution during the acquisition period. In other words, the comparison of the amplitude of resonance broadening among the spectra allowed us to establish a ranking that matched the ranking of K_d values obtained by SPR and ITC (K_d 12mer > 14mer > 20mer > 15mer > 32mer). Therefore, these experiments confirmed that the 32mer is the peptide with the highest affinity to 14-3-3, followed by the 15mer, the 20mer, the 14mer, and the 12mer. In addition, the plots in Figure 3e showed that I/I_0 profiles obtained by NMR are similar for all the peptides, establishing that the binding interface is globally conserved. This result also suggested that extra contacts that could be established by the longer peptides with the protein when compared to the 12mer are unlikely sufficient by themselves to explain the measured variation in the K_d. This observation led us to consider that the basis for the differences in the binding affinities may not rely only on the bound peptide in the complex, but also on the properties of the free peptide.

NMR Spectroscopic Studies on the Structure of 12mer and 15mer. Although the NMR interaction experiments confirmed the ranking of relative affinities observed for the peptides by both ITC and SPR, they did not explain the differences in affinities, as contact surfaces were not modified from one peptide to the other. As the difference could not be found at the interface, we reasoned that it could arise from the conformational properties of the peptide itself, which could also affect the interaction. To prove this hypothesis, we performed a set of NMR experiments directed at the 12mer and 15mer free peptides, in order to investigate whether distinct conformational propensity could be observed and potentially be linked to the differences in the binding affinity to 14-3-3σΔC17. The recorded spectra, based on ^{1}H and natural abundance of ^{15}N or ^{13}C of the unlabeled peptides, allowed us

DOI: 10.1021/acschembio.9b00893
ACS Chem. Biol. 2020, 15, 262−271

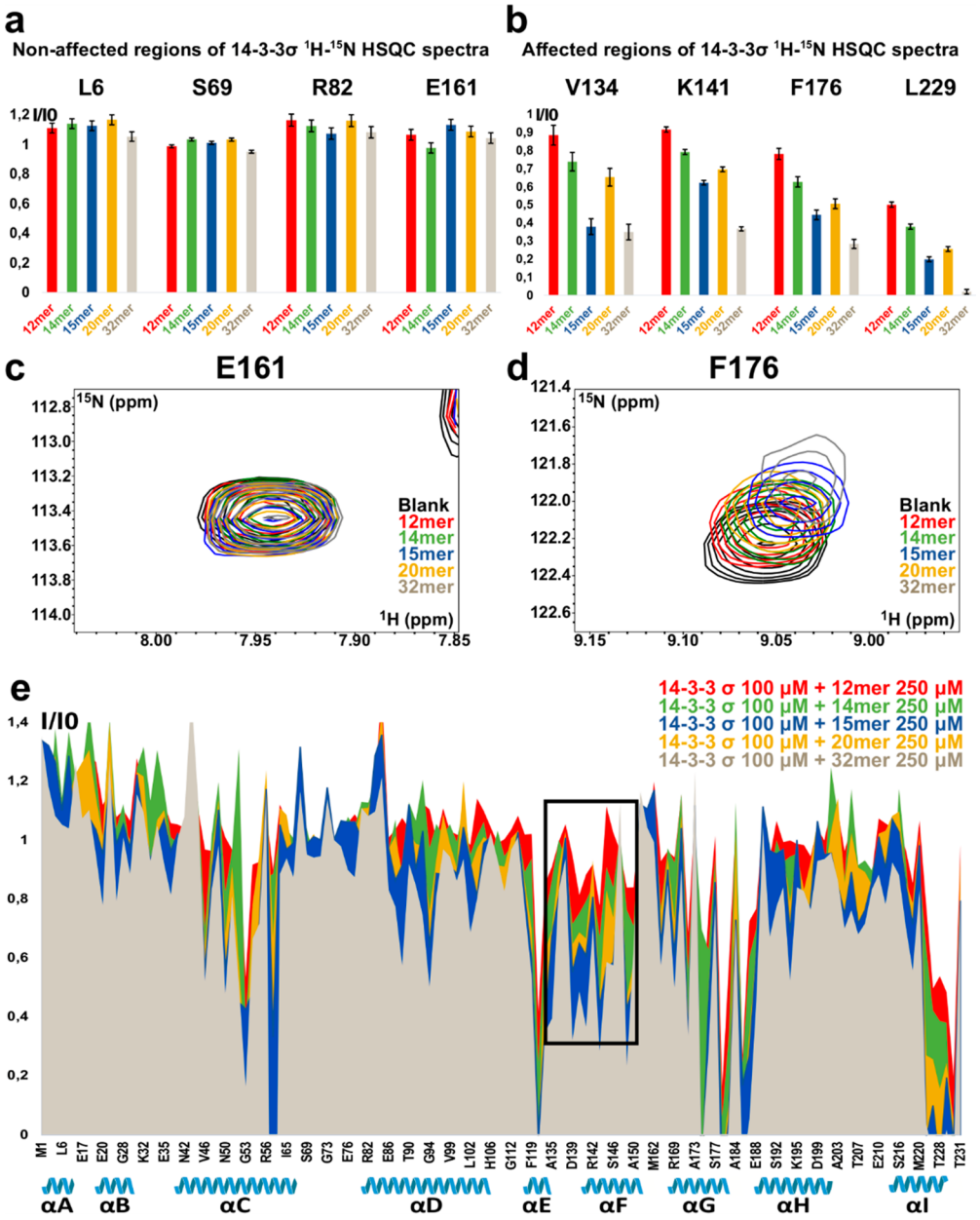

Figure 3. Interaction of p53 peptides with 14-3-3σΔC17. Plot of the ratios of the bound (I)/free (I0) $^{1}H-^{15}N$ HSQC correlation peak intensities of individual resonances corresponding to residues of the protein, remote from the interaction site (a) or close to the interaction site (b), in the presence of 12mer (red bar), 14mer (green bar), 15mer (blue bar), 20mer (yellow bar), and 32mer (gray bar). Error bars of I/I_0 ratios were calculated based on the maximum noise estimate of each spectrum. The intensities of peaks shown in panel (c) were not altered when 14-3-3σΔC17 was exposed to any of the peptides (a). On the contrary, in panel (d), broadening of resonances due to the presence of each peptide lead to decrease of I/I_0 ratios (b), with the highest decrease for the 32mer, followed by the 15mer, the 20mer, the 14mer, and the 12mer. (c) Enlarged region of overlaid $^{1}H-^{15}N$ HSQC spectra showing an individual resonance corresponding to residue E161 (remote from the binding site, see panel a) of in black: 14-3-3σΔC17 and overlaid in red, green, blue, yellow, gray: 14-3-3σΔC17 in the presence of the 12mer, 14mer, 15mer, 20mer, and 32mer peptide, respectively. (d) Same as (c) for an individual resonance corresponding to residue F176 (close to the binding site, see panel b). Note that the extent of the chemical shift perturbation caused by the peptides was higher for the 32mer, followed by the 15mer, the 20mer, the 14mer, and the 12mer. The intensities of peaks shown in panel (c) were not altered when 14-3-3σΔC17 was exposed to any of the peptides (a). On the contrary, in panel (d), broadening of resonances due to the presence of each peptide lead to a decrease of I/I_0 ratios (b), with the highest decrease for the 32mer, followed by the 15mer, the 20mer, the 14mer, and the 12mer. (e) Plot of the ratios of the bound (I)/free (I_0) $^{1}H-^{15}N$ correlation peak intensities of 14-3-3σΔC17 (y-axis) versus the amino acid sequence (x-axis) in the presence of 12mer (red plot); 14mer (green plot); 15mer (blue plot), 20mer (yellow plot); and 32mer (gray plot). A total of 136 correlation peak intensities are shown. The x axis is not proportional. The helices of 14-3-3σΔC17 are identified below the x-axis. The squared region of the plot best exemplify the gradual increase in broadening of specific resonances in 14-3-3σΔC17 spectra, induced by the series of peptides. The concentration of 14-3-3σΔC17 in all the experiments was 100 μM and the concentration of peptide, 250 μM.

to obtain chemical shift assignments (Tables S1 and S2). The chemical shift values of $^{13}C\alpha$ and $^{13}C\beta$ were first used as an indication of the presence of local secondary structure, as these values are linked to the dihedral angles of each amino-acid

DOI: 10.1021/acschembio.9b00893
ACS Chem. Biol. 2020, 15, 262−271

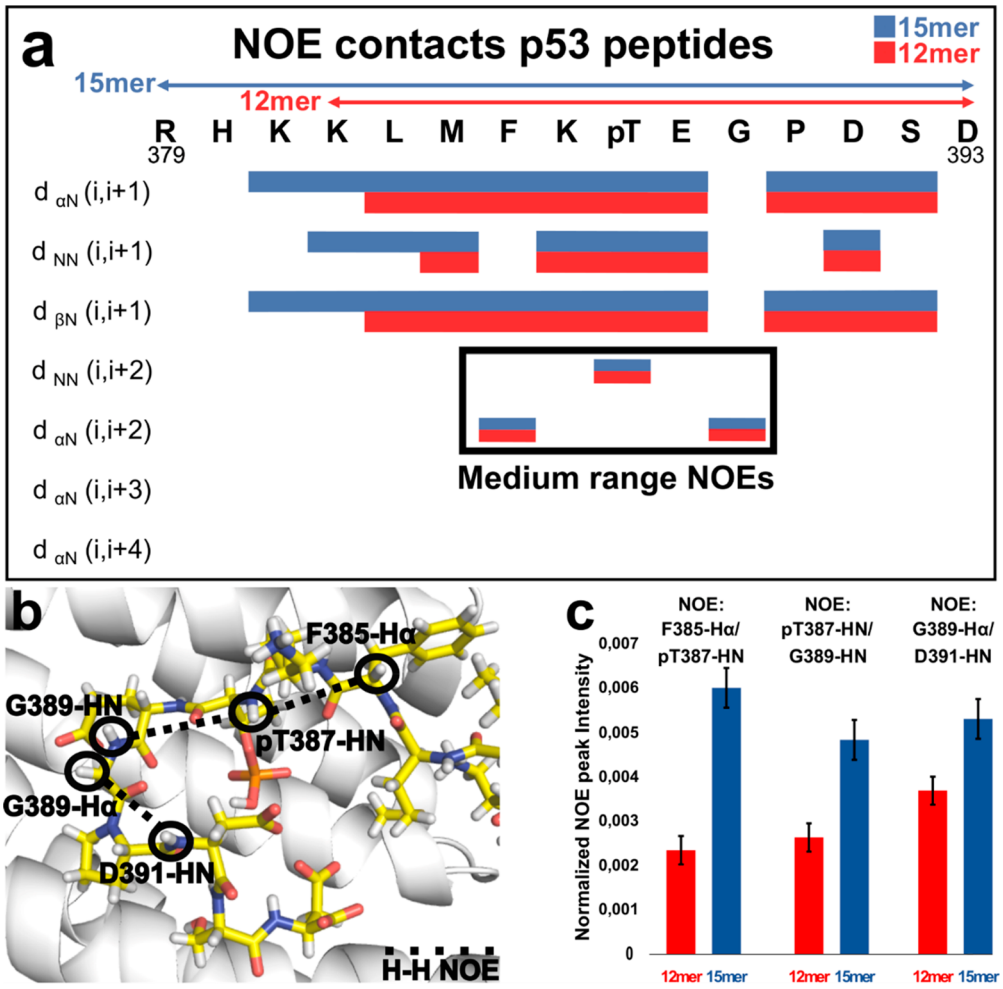

Figure 4. Peptides adopt a conformation in solution that corresponds to the 14-3-3 binding conformation. (a) NOE summary diagram for 15mer (in blue) and for 12mer (in red) in 100 mM sodium phosphate, 50 mM NaCl, pH 6.8 at 4 °C. NOE intensities were classified as strong (for sequential NOEs) and weak (for nonsequential NOEs) and are proportional to bar thickness. Sections of NOESY spectra are presented in S5 and S6. (b) Detailed view of the amphipathic binding groove of 14-3-3σ (white cartoon representation) in the presence of 12mer (yellow sticks representation) on the crystal structure (PDB ID: 5MHC).[27] The atoms involved on the midrange NOEs are surrounded by a black circle and identified on the structure. The NOE profile of the peptides in solution seems well correlated with the position of the atoms on the crystal structure. (c) Plot of the normalized intensities of the NOE correlation peaks for medium range NOEs (F385-Hα/pT387-HN; pT387-HN/G391-HN; G391-Hα-D393-HN) for the 12mer (red bars) and for the 15mer (blue bars). The intensities of the peaks are normalized to the intensity of the diagonal peak on the NOESY spectrum corresponding to the HN of pT387. The most intense cross-peak for each medium-range NOE was used for the intensity calculation. Error bars of I/I_0 ratios were calculated based on the maximum noise estimate of each spectrum. The bars show that the intensities of all the medium-range NOEs are higher for the 15mer.

residue. Calculation of the secondary structure propensity scores (Figure S4) showed a tendency to adopt β-strand conformation (negative scores), although the chemical shift values clearly indicated that both peptides had a dynamic disordered structure. The SSP score profile along the sequence of the 12mer and 15mer peptides was found to be different—an unexpected observation for short peptides with high dynamics that usually leads to averaging of the NMR parameters. An additional NOESY spectrum was thus used to search for NOE contacts between the atoms of the peptides in solution, indicative of spatial proximity (Figure 4a) and potential local dynamic structuration. Interestingly, in both peptides, the presence of three NOEs between protons of nonsequential residues confirmed that their structures are not completely disordered (Figure 4a). NOE cross-peaks could be observed between the Hα of F385 and the HN of pT387, between the HN of pT387 and the HN of G389, and finally between the Hα of G389 and the HN of D391 (Figure 4a). These data suggested that among the multiple conformations experienced by these predominately disordered peptides in solution, there was formation of a dynamic turn, whose prevalence is however high enough to be detected by NMR. This NOE profile seemed well-correlated with the position of these atoms in the crystal structure of 14-3-3σ in complex with the 12mer (Figure 4b). This fact suggested that in solution a population of the peptides has a bended conformation that is compatible with the one observed in the crystal structure (PDB ID: 5MHC).[21]

We observed in the dynamic ensemble of peptide conformations a tendency to adopt a bended conformation, involving residues pT387 to D391. In addition, β-strand propensity is observed along the peptide sequence. This conformational preference is in line with the distribution of charges across the sequence, with four positive charges in the first N-terminal half matched by four negative charges in the C-terminal half, including pT387, in the 15mer. The presence of

DOI: 10.1021/acschembio.9b00893
ACS Chem. Biol. 2020, 15, 262−271

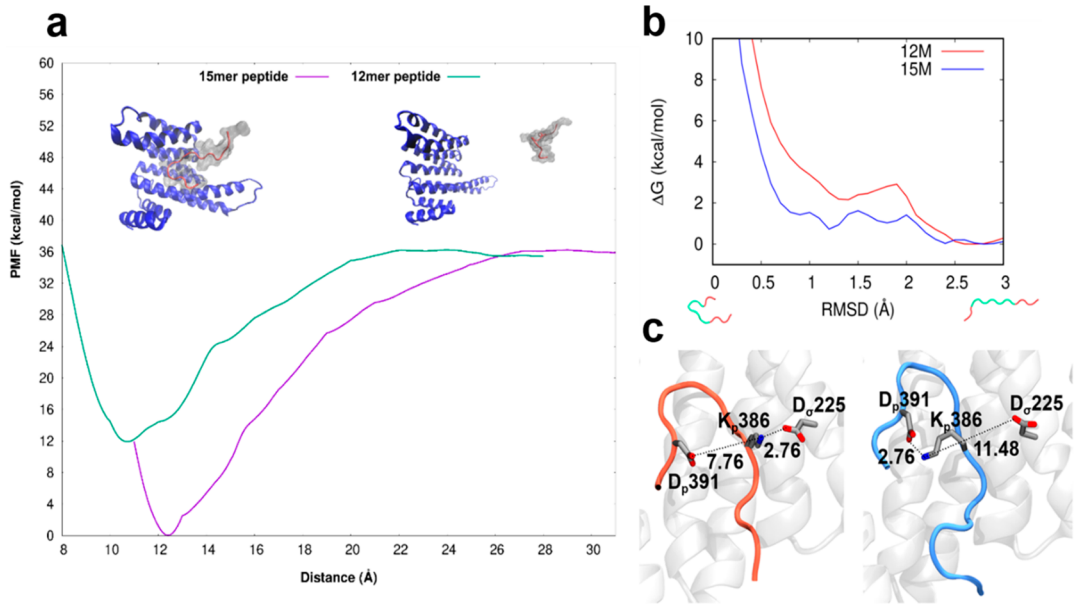

Figure 5. (a) Potential of mean force (PMF) showing the binding free energy contribution from pulling the peptides away from the protein while constraining the geometries to the bound conformations. The PMFs are obtained as a function of the distance between the center of masses of the protein and the peptides. The PMFs show that the work needed to detach the 15mer is ∼12 kcal/mol higher than the work for detaching the 12mer. This contribution, combined with −10.1 kcal/mol to account for the conformational constraints of the 12mer and the 15mer (Table S3), renders a nearly 2 kcal/mol difference between the predicted affinities of the 12mer and the 15mer for 14-3-3σ. (b) PMF profile for the conformational change between the bound-like and the extended conformation of the peptides. The bound-like and extended conformations for the 12mer are shown below the RMSD axis. The backbone atoms of residues colored in green (Kp386 to Dp391) are used for the calculation of the RMSD. (c) Conformations adopted by the 12mer (red) and 15mer (blue) peptides during the MD simulations of the peptides with 14-3-3σ. The intrapeptide interaction between Kp386 and Dp391 in the 15mer contributes to stabilize the turn conformation. Distances are in Å, and 14-3-3σ is shown in gray.

the turn suggested that electrostatic contributions allowed the peptide to fold on itself, forming a dynamic short β-sheet. The 12mer, in contrast, lacks the three first positive charges, resulting in a charge imbalance that could explain the observed smaller propensity to adopt the turn conformation. Accordingly, the normalized intensities of the three medium range NOEs that identify the turn were higher for the 15mer than for the 12mer (Figure 4c), suggesting that the population of this bended conformation in solution is higher on the 15mer than on the 12mer.

Energy Profiles of p53 12mer and 15mer Peptides Binding to 14-3-3σ. To gain further insights into the dynamic behavior of the 12mer and 15mer peptides, we performed a series of in silico biomolecular simulations. First, the binding free energies of both peptides to 14-3-3σ were calculated using extended-system adaptive biasing force (eABF) calculations.[22] The values for 12mer and 15mer binding respectively were found to be −6.6 and −8.7 kcal/mol and thus corroborate the trend in affinity obtained from the biophysical experiments. The lower binding affinity of the 12mer by ∼2 kcal/mol, with respect to the 15mer, is a reasonable value considering that the 15mer is a moderate binder (K_d = 25.7 μM). In addition, the 12mer is capable of cocrystallizing with the protein, thus suggesting that the 12mer also binds 14-3-3σ.

The potential of mean force (PMF) required to dissociate the ligands from the protein was calculated. The PMF values were obtained as a function of distance between peptide and 14-3-3σ, where the protein-bound peptide conformation was retained throughout (Figure 5a, see also Figure S7 and Table S3). The difference between the PMF profiles shows that even when the binding interface of both peptides is the same, the work needed to detach the 15mer peptide is 12 kcal/mol higher than for the 12mer. The large free energy change, favoring the 15mer, is however partially mitigated by the work needed to fix each peptide in its bound conformation when they are transferred to the bulk solvent. This can be quantified by the free energy difference between the conformational (and orientational) constraints (ΔGc) applied to both peptides in their bound geometries, which is $\Delta\Delta G_c = \Delta Gc_{12m} - \Delta Gc_{15m} =$ −10.1 kcal/mol. Thus, combining both contributions, the bound state geometry of the 15mer in solution is favored by about 2 kcal/mol over the 12mer, as mentioned above. This is in very good agreement with the NMR data showing that, in solution, the 15mer retains more population of its bound geometry than the 12mer.

The NMR experiments and the simulations of the 14-3-3σ−peptide complexes suggest that the binding free energy of the peptides depends on the relative free energy content of the bound-like peptide conformation in solution. Thus, we also studied the relative energetic content of the peptide structures in water using the eABF formalism.[22] The root-mean-square-deviation (RMSD) value of the backbone atoms of residues Kp386 to Dp391 was used as the collective variable, and the 14-3-3σ bound conformation was taken as the reference structure (Figure 5b). The sharp increase in the PMF at low RMSD values with respect to the bound-like conformation indicates a high energy content of these structures in the unbound state. On the other hand, the analysis of the PMF in the region above RMSD = 1 evidence that there is no significant free energy barrier among most of the peptide conformations in solution. This observation supports the partly

DOI: 10.1021/acschembio.9b00893
ACS Chem. Biol. 2020, 15, 262−271

disordered nature of these peptides as also suggested by the NMR studies.

Molecular Dynamics (MD) Simulations of the p53 Peptide-14-3-3σΔC17 Complexes. MD simulations of both the 12mer and the 15mer interacting with 14-3-3σ were performed (three independent replicas of 250 ns each, for both systems). In agreement with the calculated binding free energies, both the 12mer and the 15mer remain bound to 14-3-3σ during the trajectories. Binding of the peptides to 14-3-3σ involves the formation of a loop comprising residues K_p386 to D_p391 (peptide residues are identified with the subscript p and residues of 14-3-3σ with the σ subscript). This loop is conserved during the MD simulations as indicated by the small RMSD values adopted by the backbone atoms of residues K_p386 to D_p391 (Figure S8). The simulations showed that the residues of 14-3-3σ in contact with the peptides are similar in both cases (Figure S9), in agreement with the NMR observations. Binding of both peptides to 14-3-3σ is mainly driven by the positioning of pT_p387 in the binding site. There, pT_p387 establishes conserved salt bridges with residues $K_σ$49, $R_σ$56, $R_σ$129, and $Y_σ$130. In addition, E_p388 forms a salt bridge with $K_σ$122 (Table S4), and F_p385 remains docked in a small cavity formed by $V_σ$178, $Y_σ$181 $E_σ$182, $L_σ$229, and $W_σ$230. This explains why the I/I_0 ratio for $L_σ$229 experiences the changes shown in Figure 3. However, the simulations highlighted differences between the interaction profiles of the 12mer and 15mer peptides. In the case of the 12mer peptide, two additional interactions with 14-3-3σ (compared to the main interactions described above) are conserved for more than 50% of the trajectories (Table S4). The interaction between K_p382 and $E_σ$182 is found in 78% of the conformations and effectively restricts the movement of the N-terminus of the 12mer peptide. The salt bridge between K_p386 and $D_σ$225 is found in 56% of the conformations. Importantly, intrapeptide interactions are scarce for the 12mer. By contrast, the interaction between K_p382 and $E_σ$182 is considerably less favored in the 15mer (Table S4). Furthermore, K_p386 of the 15mer preferentially establishes an intrapeptide interaction with D_p391 instead of the peptide−protein interaction with $D_σ$225 (Figure 5c). This suggests that the introduction of additional residues at the N-terminus of the 15mer allows a redistribution of the network of interactions, increasing the propensity of the 15mer to adopt a turn conformation. This difference in the network of interactions may explain the different binding affinities of the peptides.

R379A and K386A p53 Peptide Mutations Negatively Impact on Binding Affinity. In the biophysical experiments, R_p379 was shown to have a positive effect on the binding affinity of p53 peptides. In the MD simulations, R_p379 explores an area around the binding cleft establishing contacts with $E_σ$182, $D_σ$225, and $T_σ$231. The populations of conformations showing distances below 4 Å for the interaction of R_p379 with $E_σ$182, $D_σ$225, and $T_σ$231 are 32%, 3%, and 9%, respectively. In addition, an intrapeptide interaction between R_p379 and D_p393 was found in 5% of the structures during the 15mer-14-3-3σ simulations. On the contrary, the N-terminal K_p382 of the 12mer does not interact with D_p393. Thus, R_p379 is likely important for both protein−peptide and intrapeptide interactions that lead to the enhanced affinity of the 15mer peptide. To provide further experimental confirmation of this, the binding affinities of 15mer peptides with mutations to these key residues (R_p379A and K_p386A) were determined by SPR. This data showed that the R_p379A and K_p386A mutations led to a 28% and 13% decrease in binding affinity respectively (Figure 6). Thus, the interaction network identified through NMR experiments and MD simulations is indeed a crucial factor that determines the affinity of p53 peptides to 14-3-3σ.

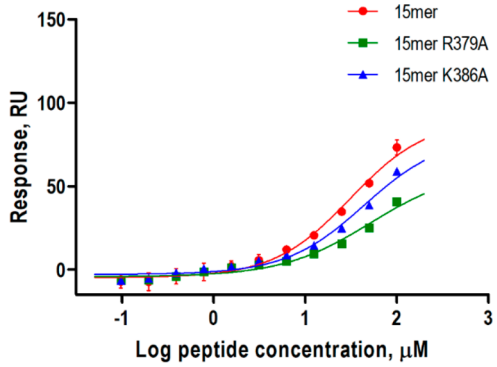

Figure 6. SPR dose−response binding curves of 15mer (K_d = 31.0 μM), 15mer R379A (K_d = 46.0 μM), and 15mer K386A (K_d = 38.8 μM) to surface-immobilized 14-3-3 protein. Alanine substitutions of R379 and K386 resulted in a decrease in binding affinities. Data presented are mean of three separate experiments.

CONCLUSIONS

Our study provides a detailed molecular and structural characterization of the important p53-14-3-3σ PPI. The eABF calculations reproduce the various types of experimental evidence of a higher binding affinity for the 15mer peptide and indicate that this ligand has higher propensity to form a loop (residues K_p386 to D_p391) with respect to the 12mer. This conclusion is strengthened by NMR NOE data that suggest a higher propensity of the 15mer to adopt a turn in the dynamic ensemble of its conformations. This conformational property allows a redistribution of the intra- and intermolecular interactions of the 15mer peptide that drives binding to 14-3-3σ. This is an important factor behind the apparently uncorrelated binding affinities of different lengths of p53 peptides as observed in SPR and ITC. These results broaden our understanding of the 14-3-3−p53 PPI and give valuable insight at the molecular level of the interaction interface. Our work reinforces the notion that conformational properties of a ligand are important parameters to take into account when designing peptidic probes for binding assays or indeed ligands to modulate PPIs.

METHODS

14-3-3σ Protein Expression and Purification. His_6-tagged full-length 14-3-3σ protein for ITC and SPR was expressed in NiCo21 (DE3) competent cells with a pProExHTb plasmid and purified using Ni^{2+} affinity chromatography according to well established procedures. 14-3-3σ protein was dialyzed against ITC buffer (25 mM HEPES pH 7.5, 100 mM NaCl, 10 mM $MgCl_2$, 0.5 mM TCEP) or a standard buffer (10 mM HEPES pH 7.5, 150 mM NaCl, 0.1% Tween 20).

The $^{15}N^{13}C^2H$ labeled 14-3-3σΔC17 protein for NMR studies was expressed in *Escherichia coli* BL21 (DE3) cells transformed with a pProExHtb vector carrying the cDNA to express an N-terminally His_6-tagged human 14-3-3σΔC17. A 20 mL preculture in *Luria−Bertani* (LB) medium containing 100 mg/L ampicillin was grown overnight at 37 °C and was used to inoculate 1 L of deuterated M9 minimal medium supplemented with 2 g/L $^{13}C_6^2H_7$ glucose, 1 g/L ^{15}N ammonium chloride, 0.4 g/L Isogro $^{15}N^{13}C^2H$ powder - growth

DOI: 10.1021/acschembio.9b00893
ACS Chem. Biol. 2020, 15, 262−271

medium (Sigma-Aldrich), and 100 mg/L ampicillin. The culture was grown at 37 °C to an OD_{600} of 0.9 and induced with 0.5 mM isopropyl-β-D-thiogalactopyranoside (IPTG). Incubation was continued for 15 h at 28 °C. Cells were harvested by centrifugation, and the protein was then purified by affinity chromatography using a Ni-NTA column (GE Healthcare). The N-terminal His_6-tag was then cleaved by the tobacco etch virus (TEV) protease for 2 h at 20 °C, followed by 12 h at 4 °C, while being dialyzed against 100 mM sodium phosphate and 50 mM NaCl, pH 6.8 (NMR buffer). The molar ratio between 14-3−3$\sigma\Delta$C17 and TEV protease was 50:1. The 14-3-3$\sigma\Delta$C17 protein without His_6-tag was collected in the flow-through of a Ni-NTA column, using NMR buffer for the elution, while the uncleaved fraction and the His_6-tag peptide were retained on the column.

Peptide Synthesis and Purification. p53 CTD T387 phosphorylated 9mer, 12mer, 14mer, 15mer, and 20mer peptides of p53 were synthesized by Fmoc solid phase chemistry using an Intavis MultiPep RSi peptide synthesizer and purified using a preparative LC-MS on a reverse-phase C18 column (Atlantis T3 prep OBD, 5 μm, 150 × 19 mm, Waters). The purification was conducted using a 17−21% gradient of acetonitrile in water (with 0.1% trifluoroacetic acid) over 12 min at 20 mL min^{-1}. pT387 32mer peptide was purchased from AnaSpec amd 15mer R379A and K386A pT387 peptides were purchased from GenScript. Peptide sequences are summarized in Table 1. LC-MS analysis for 12mer, 14mer, 15mer, and 20mer peptides is provided in the Supporting Information.

Table 1. Peptide Sequences

peptide	sequence
9mer	H_2N -FK(pT)EGPDSD- COOH
12mer	H_2N -KLMFK(pT)EGPDSD- COOH
14mer	H_2N -HKKLMFK(pT)EGPDSD- COOH
15mer	H_2N -RHKKLMFK(pT)EGPDSD- COOH
15mer R379A	H_2N -AHKKLMFK(pT)EGPDSD- COOH
15mer K386A	H_2N -RHKKLMFA(pT)EGPDSD- COOH
20mer	H_2N -GQSTSRHKKLMFK(pT)EGPDSD- COOH
32mer	H_2N -SRAHSSHLKSKKGQSTSRHKKLMFK(pT) EGPDSD- COOH

Isothermal Titration Calorimetry (ITC). Isothermal titration calorimetry (ITC) experiments were performed using Malvern MicroCal ITC200 and MicroCal Auto-iTC200 instruments. Binding experiments were carried out at 25 °C in ITC buffer (25 mM HEPES pH 7.5, 100 mM NaCl, 10 mM $MgCl_2$, 0.5 mM TCEP). 1 mM (12mer, 15mer, 20mer) or 2 mM (9mer, 14mer, 32mer) solutions of p53 peptide were titrated into the sample cell containing 0.1 mM (12mer, 15mer, 20mer) or 0.05 mM (9mer, 14mer, 32mer) of 14-3-3σ. 1% v/v DMSO was added to both cell and titrant. The dissociation constant (K_d), binding enthalpy (ΔH) and entropy (ΔS), Gibbs free energy (ΔG), and binding stoichiometry (n) were calculated using nonlinear least-squares regression analysis with Origin 7.0.

Surface Plasmon Resonance (SPR). SPR experiments were performed using a Biacore 3000 optical biosensor equipped with research-grade HC200 sensor chip (XanTec Bioanalytics). All measurements were carried out at 25 °C at a flow rate of 20 μL/min. Immobilization of 14-3-3ζ protein was conducted in sodium acetate buffer (pH 5) and peptide titration experiments in $HBSP^+$ buffer (0.01 M HEPES pH 7.4, 0.2 M NaCl, 0.05% v/v surfactant P20). The carboxylate groups on the surface were activated with a 1:1 mixture of 0.4 M *N*-ethyl-*N*′-(3-(dimethylamino)propyl)-carbodiimide (EDC) and 0.1 M *N*-hydroxysuccinimide (NHS). His_6-tagged 14-3-3ζ (3 μM) was covalently immobilized onto the activated surface with a density of 6000 RU (6 ng/mm^2). Remaining active groups were blocked by injection of 0.5 M ethanolamine in $HBSP^+$ buffer. Experiments with alanine-substituted peptides were performed using Biacore X100 machine. Measurements were conducted at a flow rate of 10 μL/min. Binding of p53 peptides to 14-3-3ζ was measured by injecting 2-fold serial dilutions of peptide in the running buffer over the sensor chip for 2 min followed by a dissociation of unbound peptide for 3 min. Dissociation constants (K_d) were calculated with GraphPad Prism 7.02 Software using a nonlinear regression analysis.

$^1H-^{15}N$ HSQC Spectroscopy on $^{15}N^{13}C^2H$ Labeled 14-3-3$\sigma\Delta$C17. $^1H-^{15}N$ TROSY-HSQC (transverse relaxation optimized spectroscopy-heteronuclear single quantum coherence spectroscopy) spectra were acquired in 3 mm tubes (sample volume 200 μL) using a 900 MHz Bruker Avance spectrometer, equipped with a cryoprobe. The spectra were recorded with 3426 complex data points in the direct dimension and 128 complex data points in the indirect dimension, with 300 scans per increment, at 32 °C, in a buffer containing 100 mM sodium phosphate, 50 mM NaCl, pH 6.8, 1 mM DTT, EDTA-free protease inhibitor cocktail (Roche, Basel, Switzerland) and 10% (v/v) D_2O. The experiments were performed with samples containing 100 μM $^{15}N^{13}C^2H$ labeled 14-3-3$\sigma\Delta$C17 in the presence or in the absence of 250 μM p53 peptide. The experiments were performed on the 12mer, 14mer, 15mer, 20mer, and 32mer peptides. The reference for the ^1H chemical shift was relative to trimethylsilyl propionate. Spectra were collected and processed with Topspin 4.0 (Bruker Biospin, Karlsruhe, Germany) and analyzed with Sparky 3.12 (T. D. Goddard and D. G. Kneller, SPARKY 3, University of California, San Francisco). The backbone resonance assignments of 14-3-3$\sigma\Delta$C17 are recorded in the Biological Magnetic Resonance Database (http://www.bmrb.wisc.edu/) under the BMRB accession number 27563.[23]

NMR Spectroscopy on 12mer and 15mer Peptides. All 2D NMR spectra of natural abundance 12mer and 15mer peptides were acquired in a buffer containing 100 mM sodium phosphate, 50 mM NaCl, pH 6.8, and 10% (v/v) D_2O at 4 °C using a 600 MHz Bruker Avance I spectrometer equipped with a CPQCI cryoprobe. The spectra were recorded in Shigemi NMR tubes at a peptide concentration of 2.25 mM and in the absence of 14-3-3. The set of NMR experiments consisted of a $^1H-^{15}N$ HSQC (^{15}N natural abundance), a $^1H-^{13}C$ HSQC (^{13}C natural abundance), a TOCSY (total correlation spectroscopy) and a NOESY (nuclear overhauser effect spectroscopy). $^1H-^{15}N$ HSQC experiments were recorded with 2048 complex data points in the direct dimension and 64 complex data points in the ^{15}N dimension with 300 scans per increment. $^1H-^{13}C$ HSQC experiments were recorded with 1440 complex data points in the direct dimension and 128 complex data points in the ^{13}C dimension with 32 scans per increment. TOCSY and NOESY spectra were acquired with 8192 × 512 complex data points, with a recycle delay of 1s and with 32 and 64 scans per increment, respectively. The mixing times were 69 ms for the TOCSY and 400 ms for the NOESY experiments. The reference for the ^1H chemical shift was relative to trimethylsilyl propionate. Spectra were collected and processed with Topspin 3.5 (Bruker Biospin, Karlsruhe, Germany) and analyzed with Sparky 3.12 (T. D. Goddard and D. G. Kneller, SPARKY 3, University of California, San Francisco). The assignment of chemical shifts of peptides reached a completeness of 88% for the 12mer and 86% for the 15mer concerning the chemical shift values of ^{15}N, $^1H^N$, $^1H\alpha$, $^1H\beta$, $^{13}C\alpha$, and $^{13}C\beta$. The secondary structure propensity (SSP) scores[24] were calculated for both peptides based on $^{13}C\alpha$ and $^{13}C\beta$ chemical shift values. Random coil chemical shift values used for the calculation of the SSP score were taken from RefDB database.[25] The $^{13}C\alpha$ and $^{13}C\beta$ random coil chemical shift values for phosphorylated threonine used for the calculation of the SSP scores were taken from the literature.[26]

Computational Details. The starting point for the molecular dynamics simulations (MD) was the crystal structure of the complex between the p53 C-terminal 12mer pT387 phosphopeptide and 14-3-3σ (PDB code: 5MHC).[21] The 15mer phosphopeptide was also considered. All missing residues in 14-3-3σ were built using the program Modeler 9.15.[27] The 15mer peptide was bound to 14-3-3σ similar to the 12mer. The phosphorylated threonine residue was simulated with charge −2 in the phosphate group since the binding site in 14-3-3σ contains several positively charged residues near the phosphate group. The systems were placed in a water box with 20 Å distance between the protein and the walls of the box. The TIP3P

DOI: 10.1021/acschembio.9b00893
ACS Chem. Biol. 2020, 15, 262−271

water model was used in all simulations.[28] All systems were neutralized. MD simulations were carried out in the NPT ensemble for 250 ns and three independent replicas of each simulation were performed with CHARMM36m as force field.[29] A time step of 2 fs was employed. The cutoff used was 12 Å, while the pair list distance was set to 13.5 Å. All simulations were performed with NAMD 2.12.[30] The analysis of the trajectories was performed with VMD.[31] The cutoff used for the analysis of the distances was 4 Å, while for the RMSD was 0.8 Å.

In the eABF[22] calculations, default values for the force contacts and harmonic constraints were used, and the tool BFEE[32] was employed for the setup and analysis of the calculations. The ligand pulling contribution to the free energy was obtained by splitting the trajectory into 10 windows, each covering an increment of 2 Å in the distance between the center of masses of the protein and the peptide. The convergence analysis of the windows was carried out by monitoring the norm of the PMF profiles at increasing trajectory times. The corrected *z*-averaged restraint estimator (CZAR) was used to obtain all the PMFs for the binding free energy analysis.[33] To analyze the behavior in water of the two peptides, we divided the collective variable in six equal windows of 0.5 Å and set the bin width to 0.1 Å. The collective variable was the RMSD of the backbone atoms of residues Kp386 to Dp391 (Figure S10, Supporting Information). Each window was simulated for 20 ns (Figure S11, Supporting Information). A total of 100 samples were taken in each bin before applying the force. The extended Lagrangian[34] formalism was used, and the final PMF was obtained with the CZAR estimator.[33]

■ ASSOCIATED CONTENT

Supporting Information

The Supporting Information is available free of charge at https://pubs.acs.org/doi/10.1021/acschembio.9b00893.

ITC titration curves of p53 peptides; $^{1}H-^{15}N$ TROSY-HSQC spectra of 14-3-3σΔC17 in the presence of p53 peptides; mapping of the crystal structure of 14-3-3σΔC17 in complex with 12mer; ^{15}N, ^{1}H, and ^{13}C Chemical shift values of 12mer and 15mer; SSP scores of p53 peptides; NOE contacts in 12mer and 15mer; molecular dynamics of the 14-3-3−12mer/15mer complexes; RMSD values; average distances for selected interactions; structure of the bound conformation of the 12mer peptide; time evolution of the PMF profiles for the 15mer and 12mer; LC-MS data of p53 peptides (PDF)

■ AUTHOR INFORMATION

Corresponding Authors

*(R.G.D.) E-mail: r.g.doveston@leicester.ac.uk.
*(C.O.) E-mail: c.ottmann@tue.nl.
*(H.B.) E-mail: helen.boyd@astrazeneca.com.
*(I.L.) E-mail: isabelle.landrieu@univ-lille.fr.
*(E.S.-G.) E-mail: elsa.sanchez-garcia@uni-due.de.

ORCID

Yasser B. Ruiz-Blanco: 0000-0001-5400-4427
Michael Ehrmann: 0000-0002-1927-260X
Elsa Sanchez-Garcia: 0000-0002-9211-5803
Christian Ottmann: 0000-0001-7315-0315

Author Contributions

◆A.K., J.F.N., and K.B.R. contributed equally.

Notes

The authors declare no competing financial interest.

■ ACKNOWLEDGMENTS

The research is supported by funding from the European Union through the AEGIS project (H2020-MSCA-ITN-2015, Grant Number 67555), TASPPI project (H2020-MSCA-ITN-2015, Grant Number 675179), and MSCA IEF (H2020-MSCA-IEF-2016, Grant Number 705188, R.G.D). J.F.N. and I.L. acknowledge LabEx (Laboratory of Excellence) for financial support on the scope of the DISTALZ consortium (ANR, ANR-11-LABX-009). E.S.-G. acknowledges a Plus-3 Grant of the Boehringer-Ingelheim Foundation and the computational time provided by the Computing and Data Facility of the Max Planck Society. The German Research Foundation (DFG) supported this work via the Collaborative Research Center SFB1093 (C.O., M.E., and E.S.-G.) and under Germany's Excellence Strategy RESOLV EXC2033, Project Number 390677874 (E.S.-G., infrastructure support). We acknowledge F. X. Cantrelle for assistance on NMR data acquisition. The NMR facilities were funded by the Nord Region Council, CNRS, Institut Pasteur de Lille, the European Community (ERDF), and the French Ministry of Research and the University of Lille and by the CTRL CPER cofunded by the European Union with the European Regional Development Fund (ERDF), by the Hauts de France Regional Council (contract no. 17003781), Métropole Européenne de Lille (contract no. 2016_ESR_05), and French State (contract no. 2017-R3-CTRL-Phase 1). We acknowledge support for the NMR facilities from TGE RMN THC (CNRS, FR-3050) and FRABio (Univ. Lille, CNRS, FR-3688).

■ REFERENCES

(1) Brown, C. J., Lain, S., Verma, C. S., Fersht, A. R., and Lane, D. P. (2009) Awakening guardian angels: drugging the p53 pathway. *Nat. Rev. Cancer 9*, 862−873.
(2) Liu, Y., and Kulesz-Martin, M. (2001) p53 protein at the hub of cellular DNA damage response pathways through sequence-specific and non-sequence-specific DNA binding. *Carcinogenesis 22*, 851−860.
(3) Joerger, A. C., and Fersht, A. R. (2008) Structural biology of the tumor suppressor p53. *Annu. Rev. Biochem. 77*, 557−582.
(4) Lakin, N. D., and Jackson, S. P. (1999) Regulation of p53 in response to DNA damage. *Oncogene 18*, 7644−7655.
(5) Parrales, A., and Iwakuma, T. (2015) Targeting Oncogenic Mutant p53 for Cancer Therapy. *Front. Oncol. 5*, 288.
(6) Ozaki, T., and Nakagawara, A. (2011) Role of p53 in Cell Death and Human Cancers. *Cancers 3*, 994−1013.
(7) van Heusden, G. P. (2005) 14−3-3 proteins: regulators of numerous eukaryotic proteins. *IUBMB Life 57*, 623−629.
(8) Aitken, A., Collinge, D. B., van Heusden, B. P., Isobe, T., Roseboom, P. H., Rosenfeld, G., and Soll, J. (1992) 14−3-3 proteins: a highly conserved, widespread family of eukaryotic proteins. *Trends Biochem. Sci. 17*, 498−501.
(9) Obsil, T., and Obsilova, V. (2011) Structural basis of 14−3-3 protein functions. *Semin. Cell Dev. Biol. 22*, 663−672.
(10) Mackintosh, C. (2004) Dynamic interactions between 14−3-3 proteins and phosphoproteins regulate diverse cellular processes. *Biochem. J. 381*, 329−342.
(11) Hermeking, H. (2003) The 14−3-3 cancer connection. *Nat. Rev. Cancer 3*, 931−43.
(12) Li, Z., Liu, J.-Y., and Zhang, J.-T. (2009) 14-3-3σ, the double-edged sword of human cancers. *Am. J. Transl. Res. 1*, 326−340.
(13) Dellambra, E., Golisano, O., Bondanza, S., Siviero, E., Lacal, P., Molinari, M., D'Atri, S., and De Luca, M. (2000) Downregulation of 14−3-3σ prevents clonal evolution and leads to immortalization of primary human keratinocytes. *J. Cell Biol. 149*, 1117−30.
(14) Yang, H.-Y., Wen, Y.-Y., Chen, C.-H., Lozano, G., and Lee, M.-H. (2003) 14−3-3σ Positively Regulates p53 and Suppresses Tumor Growth. *Mol. Cell. Biol. 23*, 7096−7107.

DOI: 10.1021/acschembio.9b00893
ACS Chem. Biol. 2020, 15, 262−271

(15) Lee, M.-H., and Lozano, G. (2006) Regulation of the p53-MDM2 pathway by 14−3-3σ and other proteins. *Semin. Cancer Biol. 16*, 225−234.
(16) Rajagopalan, S., Sade, R. S., Townsley, F. M., and Fersht, A. R. (2010) Mechanistic differences in the transcriptional activation of p53 by 14−3-3 isoforms. *Nucleic Acids Res. 38*, 893−906.
(17) Rajagopalan, S., Jaulent, A. M., Wells, M., Veprintsev, D. B., and Fersht, A. R. (2008) 14−3-3 activation of DNA binding of p53 by enhancing its association into tetramers. *Nucleic Acids Res. 36*, 5983−5991.
(18) Yaffe, M. B., Rittinger, K., Volinia, S., Caron, P. R., Aitken, A., Leffers, H., Gamblin, S. J., Smerdon, S. J., and Cantley, L. C. (1997) The Structural Basis for 14−3-3:Phosphopeptide Binding Specificity. *Cell 91*, 961−971.
(19) Coblitz, B., Wu, M., Shikano, S., and Li, M. (2006) C-terminal binding: An expanded repertoire and function of 14−3-3 proteins. *FEBS Lett. 580*, 1531−1535.
(20) Schumacher, B., Mondry, J., Thiel, P., Weyand, M., and Ottmann, C. (2010) Structure of the p53 C-terminus bound to 14−3-3: Implications for stabilization of the p53 tetramer. *FEBS Lett. 584*, 1443−1448.
(21) Doveston, R. G., Kuusk, A., Andrei, S. A., Leysen, S., Cao, Q., Castaldi, M. P., Hendricks, A., Brunsveld, L., Chen, H., Boyd, H., and Ottmann, C. (2017) Small-molecule stabilization of the p53 - 14−3-3 protein-protein interaction. *FEBS Lett. 591*, 2449−2457.
(22) Darve, E., Rodríguez-Gómez, D., and Pohorille, A. (2008) Adaptive biasing force method for scalar and vector free energy calculations. *J. Chem. Phys. 128*, 144120.
(23) Neves, J. F., Landrieu, I., Merzougui, H., Boll, E., Hanoulle, X., and Cantrelle, F.-X. (2019) Backbone chemical shift assignments of human 14−3-3σ. *Biomol. NMR Assignments 13*, 103−107.
(24) Marsh, J. A., Singh, V. K., Jia, Z., and Forman-Kay, J. D. (2006) Sensitivity of secondary structure propensities to sequence differences between alpha- and gamma-synuclein: implications for fibrillation. *Protein Sci. 15*, 2795−2804.
(25) Zhang, H., Neal, S., and Wishart, D. S. (2003) RefDB: a database of uniformly referenced protein chemical shifts. *J. Biomol. NMR 25*, 173−95.
(26) Bienkiewicz, E. A., and Lumb, k. J. (1999) Random-coil chemical shifts of phosphorylated amino acids. *J. Biomol. NMR 15*, 203−206.
(27) Eswar, N., Webb, B., Marti-Renom, M. A., Madhusudhan, M. S., Eramian, D., Shen, M. Y., Pieper, U., and Sali, A. (2007) Comparative protein structure modeling using MODELLER. *Curr. Protoc. Protein Sci. 50*, 2.9.1−2.9.31.
(28) Jorgensen, W. L., Chandrasekhar, J., Madura, J. D., Impey, R. W., and Klein, M. L. (1983) Comparison of simple potential functions for simulating liquid water. *J. Chem. Phys. 79*, 926.
(29) Vanommeslaeghe, K., and MacKerell, A. D., Jr. (2015) CHARMM additive and polarizable force fields for biophysics and computer-aided drug design. *Biochim. Biophys. Acta, Gen. Subj. 1850*, 861−871.
(30) Phillips, J. C., Braun, R., Wang, W., Gumbart, J., Tajkhorshid, E., Villa, E., Chipot, C., Skeel, R. D., Kalé, L., and Schulten, K. (2005) Scalable molecular dynamics with NAMD. *J. Comput. Chem. 26*, 1781−1802.
(31) Humphrey, W., Dalke, A., and Schulten, K. (1996) VMD: Visual molecular dynamics. *J. Mol. Graphics 14*, 33−38.
(32) Fu, H., Gumbart, J. C., Chen, H., Shao, X., Cai, W., and Chipot, C. (2018) BFEE: A User-Friendly Graphical Interface Facilitating Absolute Binding Free-Energy Calculations. *J. Chem. Inf. Model. 58*, 556−560.
(33) Lesage, A., Lelièvre, T., Stoltz, G., and Hénin, J. (2017) Smoothed Biasing Forces Yield Unbiased Free Energies with the Extended-System Adaptive Biasing Force Method. *J. Phys. Chem. B 121*, 3676−3686.
(34) Iannuzzi, M., Laio, A., and Parrinello, M. (2003) Efficient Exploration of Reactive Potential Energy Surfaces Using Car-Parrinello Molecular Dynamics. *Phys. Rev. Lett. 90*, 238302.

DOI: 10.1021/acschembio.9b00893
ACS Chem. Biol. 2020, 15, 262−271